physica status solidi

pss

www.interscience.wiley.com

reprints

www.pss-rapid.com

www.pss-c.com

www.pss-b.com

www.pss-a.com

WILEY-VCH

REPRINT

Phys. Status Solidi A **207**, No. 2, 291–299 (2010) / **DOI** 10.1002/pssa.200982503

physica status solidi a
www.pss-a.com
applications and materials science

Electronic and optical properties of group IV two-dimensional materials

O. Pulci*[,1], P. Gori[2], M. Marsili[1], V. Garbuio[1], A. P. Seitsonen[3], F. Bechstedt[4], A. Cricenti[2], and R. Del Sole[1]

[1] Department of Physics, University of Rome Tor Vergata and INFM-CNR-SMC, Rome, Italy and ETSF
[2] ISM-CNR, Rome, Italy and ETSF
[3] IMPMC, Université Paris 6 et 7, CNRS, IPGP, Paris, France
[4] Institut für Festkörpertheorie und Optik, Friedrich-Schiller-Universität, Jena, Germany and ETSF

Received 21 July 2009, revised 27 August 2009, accepted 27 August 2009
Published online 6 January 2010

PACS 71.15.Mb, 71.15.−m, 71.15.Qe, 71.20.−b, 78.20.Bh

* Corresponding author: e-mail olivia.pulci@roma2.infn.it, Phone: +39-06-72594548, Fax: +39-06-2023507

The microscopic study of complex systems has reached a high level of accuracy that allows for a deep understanding of their structure, electronic properties, and optical spectra. The theoretical investigation of surfaces is nowadays routinely done within density functional theory, for ground state properties, and, with a larger computational load, within many-body perturbation theory, for excited states properties. In this paper we present and discuss examples of calculations for group IV two-dimensional systems such as a clean silicon surface, a tin–germanium interface, graphene, and graphane, pointing out the importance of a pertinent treatment of many-body effects.

1 Introduction In the last decades, thanks to the huge increase in computer power, the theoretical study of the excited state properties of surfaces and interfaces has become feasible with a great level of accuracy, also including many-body effects. The development of the surface physics field has been driven, among other things, by the interest in semiconductor technology for electronics. A key parameter in practical applications is the electronic gap; hence the accurate knowledge of this property is of fundamental interest.

A first and most computationally affordable step in the investigation of the electronic structures of materials is performed within density functional theory (DFT) [1, 2]. As we will shortly see, most commonly, the fundamental gap is obtained as the difference between the energy of the lowest unoccupied, and highest occupied Kohn–Sham level. Even in an exact version of DFT, this method misses the contribution of the derivative discontinuity of the exchange-correlation energy functional, and, with the commonly used approximate functionals, systematically underestimates electronic gaps.

A possible route to estimate quantitatively the electronic gaps of materials is given by many-body perturbation theory (MBPT) within the so-called *GW* approximation for the self-energy [3]. As it will be shown in the next paragraphs the results at this level of sophistication are typically in very good agreement with experiments. The calculations are however much more demanding [4].

In this paper we want to show how these theoretical tools can be successfully applied to a variety of two-dimensional (2D) systems. For this purpose we have chosen specific systems as prototypes of different physical situations: clean Si(100)(2 × 1), tin–germanium (Sn–Ge) interface, graphene, and graphane.

Si(100)(2 × 1) has been chosen as the representative of clean semi-conducting surfaces. Here we review its geometry, electronic, and optical properties, focusing the attention on the importance of the inclusion of many-body effects in the description of the single-particle excitation energies.

As a second reference issue, we will describe the results concerning the electronic band structure and scanning tunneling microscopy (STM) simulated images of 1/3 monolayer (ML) Sn/Ge(111) system, representing the first stage of a metal–semiconductor interface. In particular it will be shown how many-body effects act differently on the semiconductor-related states and on the metallic ones. This fact is very important for the correct simulation of STM images and allows the determination of the adsorption geometry.

At last we will show how many-body calculations can be applied to the study of the electronic properties of two truly 2D systems such as graphene and graphane. Graphane, recently synthesized by Elias et al. [5], can be considered as the hydrogen-passivated graphene. We will show that the presence of the hydrogen atoms causes dramatic changes in the electronic structure of the system.

2 Theoretical methods In this section we review the theoretical methods employed in the calculations presented here. At first we briefly describe DFT, an exact theory for ground state calculations, and also a common starting point for other *ab initio* methods. Then going beyond standard DFT to describe excitations in materials, we will introduce, within the framework of MBPT, the *GW* approximation for the self-energy; it is an essential tool for the quantitative description of electronic properties and band gaps.

2.1 Density functional theory Density functional theory aims to solve the many-body ground state problem in terms of the one-particle electronic density alone. DFT is based on the Hohenberg and Kohn theorem [1] that states that once the interaction among the electrons is fixed and assuming only local potentials acting on the system, all the ground state properties of an interacting system are unique functionals of the electronic ground-state density alone. Taking into account the total energy as a functional of the ground-state electronic density, the ground state of the system could be in principle obtained by minimizing this functional. However, in practice, DFT calculations do not proceed through a direct total-energy minimization, but exploit the Kohn and Sham scheme [2] that leads to the set of self-consistent equations:

$$\left[-\frac{1}{2}\nabla^2_{\mathbf{r}} + v_{\text{ext}} + v_{\text{H}} + v_{\text{xc}}\right]\phi_i(\mathbf{r}) = \varepsilon_i\phi_i(\mathbf{r}), \tag{1}$$

$$n(r) = \sum\nolimits_i f_i|\phi_i(\mathbf{r})|^2, \tag{2}$$

where v_{ext}, v_{H}, and v_{xc} are, respectively, the external, Hartree, and exchange and correlation potentials and f_i is the occupation number of the state i. This set of self-consistent equations is obtained mapping the interacting system into a non-interacting one, and constraining the two systems to have the same ground-state density. The total energy functional is thus, smartly, expressed as:

$$E[n] = T_{\text{KS}}[n] + E_{\text{H}}[n] + \int \mathrm{d}\mathbf{r}\, n(\mathbf{r})v_{\text{ext}}(\mathbf{r}) + E_{\text{xc}}[n]. \tag{3}$$

T_{KS} is the kinetic energy of the non-interacting Kohn–Sham system, E_{H} is the the Hartree contribution to the total energy, and E_{xc} is the exchange-correlation energy functional. E_{xc} corresponds to the remaining part of the total energy, and it thus contains kinetic energy contributions and exchange-correlation effects beyond Hartree. Of course the most relevant approximations in the effective application of DFT act on this last term and on its functional derivative with respect to the density $v_{\text{xc}}[n]$.

Often Kohn–Sham eigenvalues ε_i and eigenfunctions ϕ_i are interpreted as electron addition and removal energies. This procedure, which is not theoretically established, gives frequently a qualitative agreement with experiments concerning, for example, band dispersions, however the band gaps are systematically underestimated and it is crucial to go beyond DFT in order to successfully describe electronic properties of materials.

2.2 Many-body perturbation theory – *GW* approximation Green's function theory is particularly suitable to study electronic properties: in fact, the poles of the single-particle Green's function are exactly at the electron addition and removal energies. For practical calculations, it is possible to obtain a set of single-particle-like equations by introducing the concept of quasi-particles (QPs) which can be viewed as real particles surrounded by their polarization cloud, due to electron–hole pairs, screening the mutual interaction. The difference between "bare" particles (subject only to the Hartree potential) and QPs is accounted for by a non-local, non-Hermitian, energy-dependent operator that is the self-energy Σ. The QP equations are:

$$H_0(\mathbf{r})\psi_n(\mathbf{r},\omega) + \int \mathrm{d}\mathbf{r}'\,\Sigma(\mathbf{r},\mathbf{r}',\omega)\psi_n(\mathbf{r}',\omega) = E_n(\omega)\psi_n(\mathbf{r},\omega), \tag{4}$$

where $H_0(\mathbf{r}) = -\frac{1}{2}\nabla^2_{\mathbf{r}} + v_{\text{ext}}(\mathbf{r}) + v_{\text{H}}(\mathbf{r})$.

Σ is the product of the Green's function G, the screened Coulomb interaction W, and the vertex function Γ: namely $\Sigma = iGW\Gamma$ [3]. The knowledge of the *exact* G, W, and Γ requires the self-consistent solution of the Hedin equations [3], an unfeasible job for realistic systems. Hence an adequate expression for Σ has to be found. In the *GW* approximation, the vertex corrections are neglected, and the self-energy is $\Sigma = iGW$. It is important to notice that in this expression we still find the *exact* G and W. In most common cases G is given by non-interacting Green's function G_0, and W is calculated at the RPA level, giving rise to the so-called G_0W_0 approximation:

$$\Sigma(1,2) = iG_0(1,2)W_0(2,1^+). \tag{5}$$

This expression can also be interpreted as the result of the first iteration of the closed-set of Hedin equations starting from a non-interacting scheme, typically the Kohn–Sham one. Keeping the vertex fixed to a delta-function, a self-consistent solution for the sub-set of the Hedin's equation concerning only G, W, and Σ, can be reached. However, also in this case, the achievement of full self-consistency is a intricate and terribly demanding task (e.g., Ref. [6]). What can be done to ease this task is to keep the QP wave-function fixed at the non-interacting level and to update the

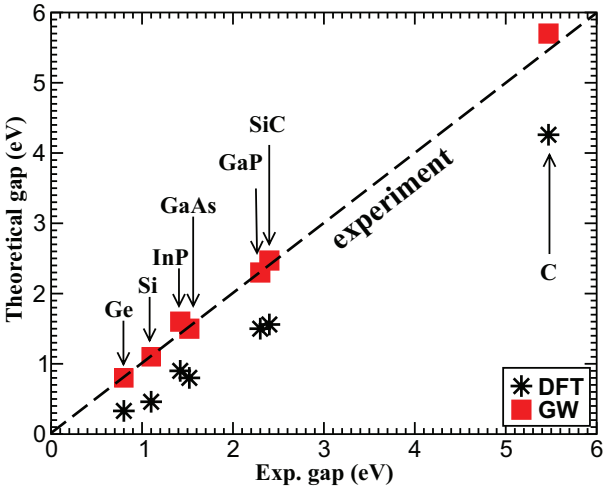

Figure 1 (online color at: www.pss-a.com) Fundamental band gap of different bulk systems calculated at the DFT–LDA and G_0W_0 level compared to the experimental value. The DFT–LDA results are always underestimating the gap and lie below the experimental line. The agreement is restored when self-energy effects within G_0W_0 are included.

quasiparticle energies in the expression of both G and W, or only in G (e.g., Ref. [7]).

In Fig. 1, it is shown how the inclusion of self-energy effects at the G_0W_0 level yields quite accurate results for one-particle excitations for several simple semiconducting bulk systems. This holds true also in a larger variety of bulk systems as shown in Ref. [8], and for semiconductor surfaces [9]. The mean absolute relative error in the determination of band gaps of the G_0W_0 method ranging around 10%, can be improved to 5% if the eigenenergies values are updated in the expression of G only [7]. In particular, for most systems, the underestimation of the band gap is removed and a quantitative agreement with photo-emission experiments is achieved for the band structure calculations.

3 Selected case studies All examples presented in the following have been studied within DFT–local density approximation (LDA) unless otherwise specified, using DFT plane-waves pseudopotential codes [10, 11]. *GW* calculations [12] have been performed using one-shot G_0W_0, with the RPA screening $\varepsilon^{-1}(\mathbf{q},\omega)$ calculated within a single plasmon pole model [13].

3.1 A clean semiconductor surface: Si(100) The Si(100) surface is the most relevant surface for what concerns microelectronic devices. As such, its accurate characterization is of paramount importance. Its atomic structure is characterized by a $c(4\times2)$ symmetry originating from silicon dimers alternatively buckled along and perpendicularly to the dimer rows [14]. At room temperature, LEED and STM display an apparent 2×1 order because of a temperature-induced flip–flop of the dimers.

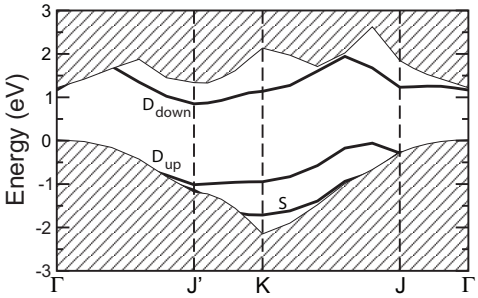

Figure 2 Calculated *GW* band structure for Si(100) (2×1).

The results presented here concern the 2×1 buckled-dimer geometry. The DFT–LDA calculations, performed on a 12 atomic layers slab, employ a 15 Ry kinetic energy cut-off and a 16 k-points sampling of the irreducible Brillouin zone (BZ). Starting from the optimized geometry, the electronic band structures and optical properties have been calculated within the single QP scheme, solving Eq. (4).

The calculated *GW* band structure for Si(100) is shown in Fig. 2. The opening of the surface states gap with respect to the DFT calculation is about 0.6 eV [15], as for bulk states. Since the silicon dimers are buckled, the surface states appearing in the band structure are related to the filled dangling bond of the silicon atom which moves upwards (D_{up}) and to the empty dangling bond of the silicon atom which moves downwards (D_{down}). The results are in good agreement with previous results obtained by Refs. [16, 17].

Further characterization of the Si(100) surface can be provided by its optical properties, in particular by its reflectance anisotropy spectra (RAS) [18], as shown in Ref. [19]. The RAS is defined as:

$$\frac{\Delta R}{R} = \frac{R_y - R_x}{R}, \tag{6}$$

where R_i is the reflectivity for light polarized along i and R is the average reflectivity. The idea underlying the reflectance anisotropy spectroscopy as a tool in surface science is the following: a cubic crystal is optically isotropic but, at the surface, this isotropy is in general broken. As a consequence, the difference in the optical response of a surface for normal incident light polarized along the two orthogonal directions is not vanishing. At a first level of approximation, then, the RAS signal is originated at the surface and it is a fingerprint of its orientation, reconstruction, and microscopic geometry. The RAS for light at normal incidence can be calculated as [20, 21]:

$$\frac{\Delta R}{R} = \frac{4\omega}{c}\,\mathrm{Im}\left[\frac{4\pi d\alpha^{hs}_{yy}(\omega) - 4\pi d\alpha^{hs}_{xx}(\omega)}{\varepsilon_b(\omega) - 1}\right], \tag{7}$$

where ε_b is the bulk dielectric function and α is the half slab polarizability [22] of a slab of width $2d$. Within the single

particle model, α takes the form:

$$\mathrm{Im}[4\pi\alpha_{ii}^{hs}(\omega)] = \frac{4\pi^2 e^2}{m^2\omega^2 A d}\sum_{\mathbf{k}}\sum_{v,c}|p_{v,c}^{i}(\mathbf{k})|^2 \times \delta[E_c(\mathbf{k}) - E_v(\mathbf{k}) - \hbar\omega], \quad (8)$$

where $p_{v,c}^{i}(\mathbf{k})$ is the matrix element of the i-component ($i = x,\ y$) of the momentum operator between initial (valence, v) and final (conduction, c) states at the point $\mathbf{k}$ in the 2D BZ, and A is the slab area. Here, we have used 128 k-points in the BZ, and summed up 50 conduction states. Being a *GW* calculations for so many states very cumbersome, and thanks to the fact that our *GW* corrections for the surface states are about 0.6 eV, i.e., the same as for bulk states, we could use the very same *GW* correction (0.6 eV) to all the states. In other words, for this surface we found that a scissor operator approximation is justified, hence we have used the calculated *GW* correction of 0.6 eV for all the transitions.

Figure 3 displays a comparison between experimental and calculated RAS for Si(100). The experiments have been described in Ref. [23]. The spectrum is dominated at high energy (4.4 eV) by a positive structure associated with the E_2 critical point; transitions at E_0' and E_1 are responsible for the structure observed around 3.4 eV. The energies of the critical points are indicated in Fig. 3. Around 1.5 eV, a negative structure is observed in the experimental spectrum as well as in the calculated one. This structure is associated with transition between π and π^* surface states delocalized along the dimer rows and it is due to the contribution of a positive intra-dimer transition and a stronger inter-negative one [24]. In the absence of QP corrections the theoretical spectra would be shifted by approximately 0.6 eV to lower energies. Thus, from the comparison of the spectra in Fig. 3, we see how the inclusion of QP energies is essential to obtain a quantitative agreement with experiments [25].

3.2 A metal–semiconductor interface: α-Sn/Ge(111) The 1/3 ML Sn/Ge(111) system (the α-phase) is characterized by Sn ad-atoms regularly located on one out of three T_4 sites of the bulk terminated Ge(111) surface, resulting in a $(\sqrt{3}\times\sqrt{3})R30^\circ$ reconstruction. Particular interest for this phase arose after the discovery of a gradual and reversible phase transition to a 3×3 reconstruction below ~220 K [26]. This transition, initially explained as a charge density wave (CDW) formation below a critical temperature, was later interpreted through a "dynamical fluctuation" model [27, 28], suggesting that the 3×3 reconstruction is the ground state and the $\sqrt{3}\times\sqrt{3}$ reconstruction, observed at room temperature, results from thermally activated rapid vertical oscillations of the Sn atoms.

The exact structure of the 3×3 reconstruction at low temperature (LT, $20\,\mathrm{K} < T < 220\,\mathrm{K}$) has been a matter of debate. Indeed, the apparent existence of two types of Sn ad-atoms, indicated by core level photo-emission spectroscopy [29], is compatible with two possible configurations of the surface: one with two Sn ad-atoms in a higher position with respect to the third one (two ad-atoms up, one down, 2U1D for brevity hereafter) and the opposite configuration, one ad-atom up, two down (1U2D). STM results alone cannot tell whether the surface configuration is 1U2D or 2U1D, because imaging empty or filled electronic states results in a honeycomb (an apparent 2U1D) image or a complementary hexagonal (an apparent 1U2D) one, respectively [26, 30], pointing to a dominant electronic rather than geometric origin of the image contrast. In order to understand which is the actual system configuration, surface-sensitive structural techniques [31–35], Sn-4d core level photoemission

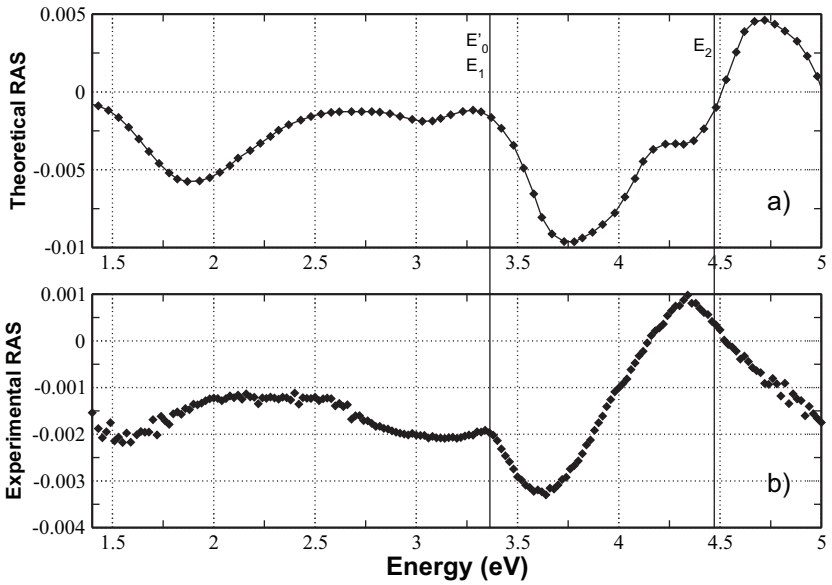

Figure 3 Comparison between calculated (a) and experimental (b) RAS of Si(100).

spectroscopy [29, 36, 37], non-contact AFM investigations [38], theoretical calculations [27, 30, 39–42] were applied, producing conflicting results.

We focus here on the LT-phase structure simulating STM images as a function of the applied voltage. First-principles calculations for the Sn/Ge(111) surface have been carried out using a repeated slab geometry consisting of six Ge layers of nine atoms each, saturated by H atoms on the bottom layer and with Sn ad-atoms on top. The geometry has been optimized within DFT in the LDA and in the generalized gradient approximation (GGA) [43]. In agreement with previous results [44], the tests we performed at the local spin density approximation (LSDA) level do not lead to substantial changes. Hence, we have neglected the spin degrees of freedom. Calculations of electron eigen-energies have been performed within a DFT + *GW* approach to allow a close comparison of theoretical and experimental results. STM images have been simulated using the Tersoff–Hamann model [45], as energy-integrated *GW*-corrected [46] local density of states at a fixed height above the sample, using an average tip-sample distance of 5 Å.

Calculations were performed on the two possible 3×3 reconstructions starting from initial configurations having a vertical buckling of 0.4 Å for both 1U2D and 2U1D systems. In both cases the relaxation converged to the same energy minimum, corresponding to a 1U2D model with a vertical buckling of 0.36 Å between up and down Sn ad-atoms. We also considered a metastable 2U1D model having a vertical buckling of 0.20 Å (a value close to the structural results reported in Ref. [35]) for comparing the resulting band structure and STM images with the ones derived from the stable 1U2D configuration. As we said previously, DFT, being a ground-state theory, in principle cannot provide information on excited-state properties as electronic band structures. The quantities that can correctly be compared with experiments are instead QP energies, that can be computed in the *GW* approximation. In many cases, DFT turns out to provide a good description of excited states, in particular when dealing with metals, where screening is very effective and *GW* corrections should be small. However, the Sn/Ge(111) system is not simply a metal but a metal/semiconductor interface. It is therefore reasonable to expect a non-trivial behavior of screening that should be in this case largely space dependent, because of both the structural and the electronic inhomogeneity of the system. We therefore calculated QP energies in the *GW* approximation. As a result, we found that the surface states bands, related to the Sn ad-atoms, are just slightly affected by self-energy effects (DFT and *GW* eigenvalues differ between −0.15 and 0.05 eV), whereas corrections for the states related to Ge are in the range −0.3/0.5 eV. The *GW* surface band structures calculated along high-symmetry directions of the 3×3 surface Brillouin zone are reported in the insets of Fig. 4a and 4b for the 1U2D and the 2U1D configurations, respectively. The three surface bands are associated to the three Sn dangling bonds: the "up" ad-atoms are characterized by a filled dangling bond while the "down" ad-atoms have partially occupied ones [44]. This is seen, for example, from the *GW* projected density of states (PDOS) at the three types of Sn ad-atoms reported in Fig. 4a and 4b. Consequently, the two upper surface bands for the 1U2D geometry are associated to 2D ad-atoms and the third band at lower energy to 1U ad-atoms. Conversely, the 2U1D band structure reported in Fig. 4b shows that the two lower bands describe

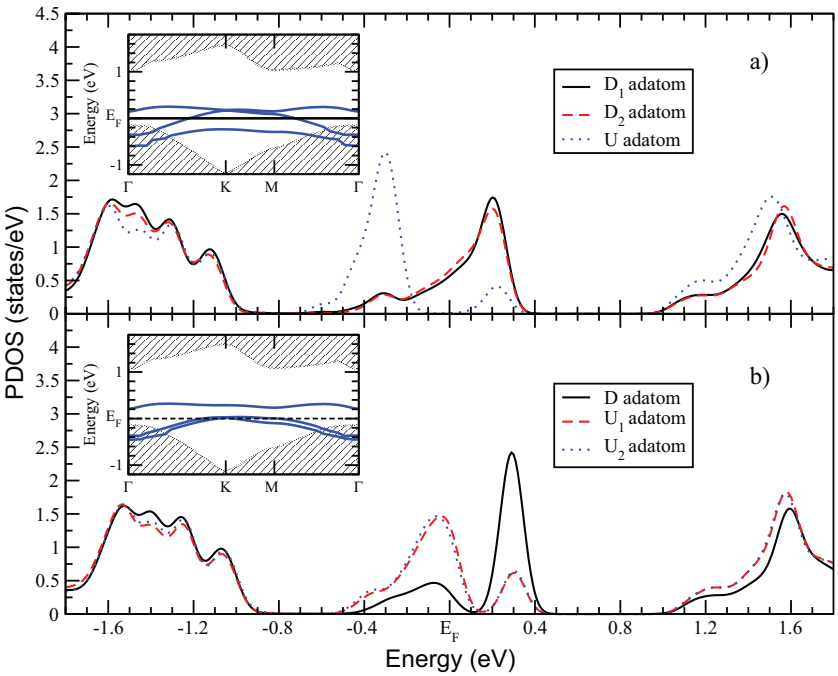

Figure 4 (online color at: www.pss-a.com) *GW* projected density of states at up and down tin ad-atoms for the 1U2D (a) and 2U1D (b) configurations. The insets show the respective *GW* surface band structures along high-symmetry directions of the 3×3 SBZ.

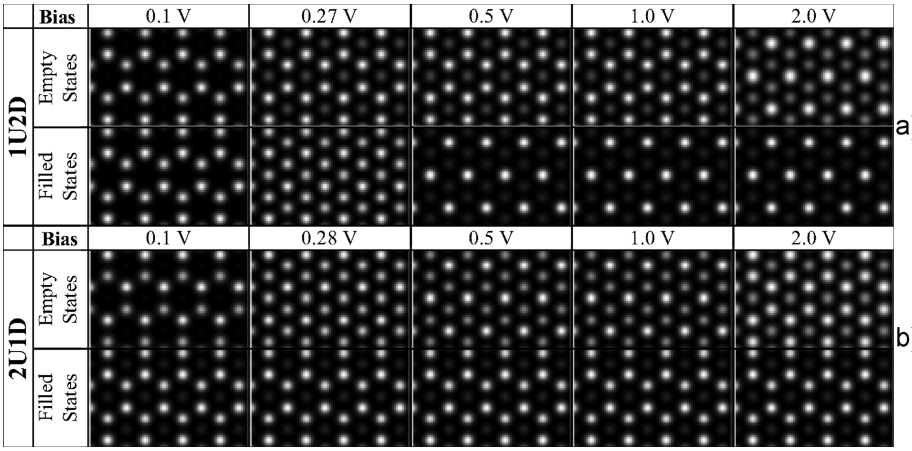

Figure 5 Simulated $5 \times 3\,\mathrm{nm}^2$ STM images for the 1U2D (a) and 2U1D (b) configurations as a function of the bias voltage.

2U ad-atoms and the third one located at higher energy describes D ad-atoms. Such PDOS curves suggest that STM images obtained with very small bias voltages should mainly show the two D ad-atoms in the 1U2D case and the two U in the 2U1D case, resulting in both cases in a honeycomb pattern. This hypothesis is confirmed by simulating STM images for the 1U2D and the 2U1D reconstructions (reported in Fig. 5a and 5b, respectively) as a function of the bias voltage V, thus performing a sort of surface electronic spectroscopy [47]. Indeed, in both cases the simulated images obtained at bias voltages lower than 0.2 V show a honeycomb pattern in both empty and filled states. Increasing the bias voltage, in the 1U2D case (Fig. 5a), the filled states images gradually revert to the expected hexagonal pattern, passing through an apparent $\sqrt{3} \times \sqrt{3}$ reconstruction at about 0.27 V, while the empty states images preserve the honeycomb pattern. As a result, the calculated images between 0.5 and 1.0 V show the well-known complementary honeycomb and hexagonal patterns (for empty and filled states, respectively) reported in many papers. Interestingly enough, a further unexpected transition from honeycomb to hexagonal is observed in the empty states images at higher bias voltage, resulting in both the filled and empty states simulated images at 2.0 V displaying a hexagonal pattern. The 2U1D simulated STM images reported in Fig. 5b show an opposite behavior: increasing the bias voltage above 0.2 V, the honeycomb to hexagonal transition occurs in the empty states images, crossing the apparently flat reconstruction at about 0.28 V, while the honeycomb pattern is maintained in the filled states images. Further increasing the bias voltage, a new hexagonal to honeycomb transition is observed in the empty states series, resulting in a honeycomb pattern for both empty and filled states images.

The analysis of the trends for the two models shows that the bias dependence of the simulated STM images of the 1U2D configuration is very similar to that reported in experiments [48, 49], whereas the 2U1D series is definitely not compatible with what observed in actual STM images. This conclusively points out a 1U2D configuration for the α-Sn/Ge(111) surface.

3.3 2D systems: graphene and graphane In the previous paragraphs we have seen how the determination of the electronic properties of a prototype surface and interface can be theoretically probed through DFT and MBPT techniques. Here we focus our attention on the truly 2D systems graphene and graphane. Thanks to its unique physical properties (for a review see, e.g., Ref. [50]), graphene is the star of the moment. Possible applications of graphene in electronic nanodevices make it desirable to render graphene semiconducting. Chemical functionalization seems to be the natural pathway to reach this goal. Recently [5, 51], hydrogenation of graphene has been achieved, giving rise to the so-called "graphane." A change of hybridization from sp^2 (graphene) to to sp^3 (graphane) is obtained (see Fig. 6) with a shrinking of the experimental C–C bond [5]. Interestingly enough, the existence of graphane

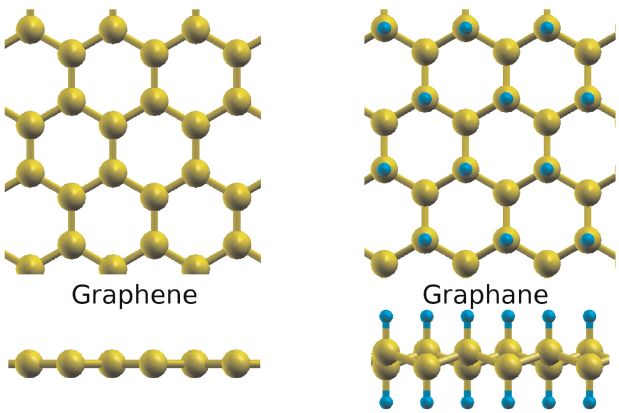

Figure 6 (online color at: www.pss-a.com) Graphene (left panel) and graphane (right panel) structures. Top view in the upper pictures and side view in the lower pictures.

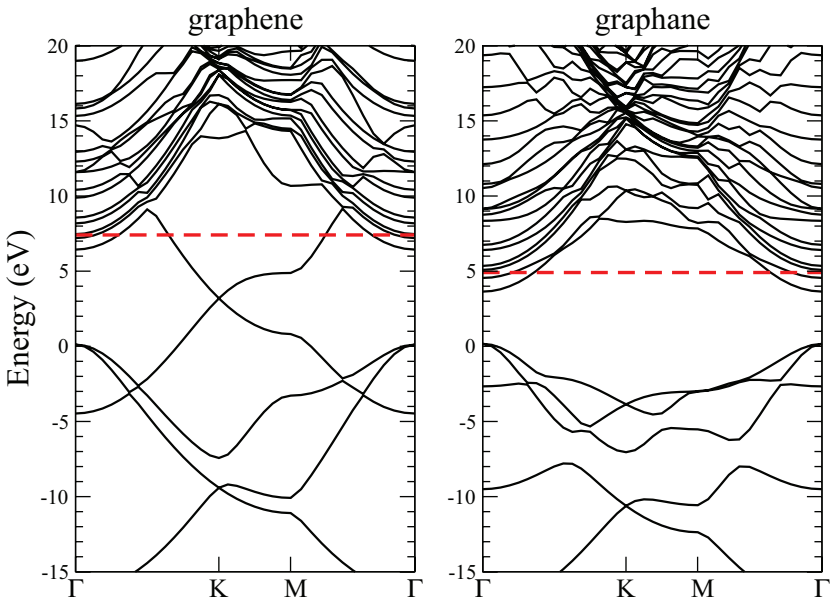

Figure 7 (online color at: www.pss-a.com) Graphene (left panel) and graphane (right panel) DFT electronic band structure. The red dashed line is the vacuum level. In graphane, the DFT gap is 3.5 eV, the *GW* gap is 5.7 eV.

has been *first* hypothesized thanks to *ab initio* calculations [52] and *then* synthesized [5, 51]. We have performed DFT–GGA [53] *ab initio* calculations of the geometry and electronic band structure of graphane [54]. Our calculations, in agreement with those of Sofo et al. [52], find a widening of the C–C bond length from 1.42 Å (graphene) to 1.54 Å (graphane). The value of 1.54 Å corresponds to the C–C distance in bulk diamond, consistently with the sp^3 hybridization, whereas the value 1.42 Å is also the C–C bond length in graphite, consistently with the sp^2 hybridization. This trend is opposite to what found in experiments [5] where graphane appears to exhibit a shrinkage of the lattice constant compared to graphene, as revealed by a structural analysis performed by transmission electron microscopy of hydrogenated graphene membranes. A possible explanation for this contradiction has been given by Legoas et al. [55] who show how breaking the H atoms up and down alternating pattern of ideal graphane, which is likely to happen in experiments, can lead to lattice contraction.

The electronic band structure of graphane is shown in Fig. 7, and compared with that of graphene. A clear metal–insulator transition, driven by H adsorption, appears, with the opening of a direct electronic gap at Γ. Our DFT value for the gap is 3.5 eV. *GW* corrections [56] strongly increase the fundamental gap of graphane giving a QP gap of 5.7 eV. It is also interesting to point out a dramatic change in the electron affinity, which goes from 4.2 eV in the metallic phase (graphene) to 1.2 eV in the insulator phase. Actually, a further reduction of the electron affinity results from *GW* calculations, giving a value as small as 0.2 eV. It seems hence that at odds with diamond-surfaces, graphene does not exhibit a negative electron affinity upon hydrogenation. More refined calculations are needed to confirm this point.

Finally, also the optical properties [57] of graphene show a dramatic change upon hydrogen adsorption (Fig. 8), with almost a complementarity in the absorption spectra. Although the DFT electronic gap of graphane is around 3.5 eV, optical absorption is almost 0 till 7 eV. Analysis of the peaks reveal that the first peak is mainly due to transitions around Γ, and the second peak to transitions around M. However in these calculations QP and excitonic effects, that can be quite important, have not been included [58].

4 Conclusions In conclusion we have shown how many-body effects, introduced within the *GW* approximation to the self-energy are crucial in the quantitative description of electronic properties of 2D systems. Their relevance is readily visible in all the different cases under

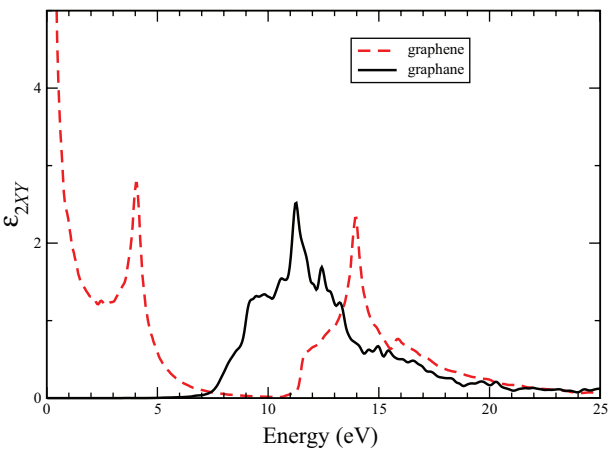

Figure 8 (online color at: www.pss-a.com) DFT-RPA imaginary part of the dielectric function of graphene (red dashed line) and graphane (black continuous line).

study covering a wide range of physical situations from a typical clean semiconducting surface (Si(001)2×1), a metal–semiconductor interface Sn/Ge, and finally truly 2D systems such as graphene and graphane.

Acknowledgements We acknowledge support from EU e-I3 ETSF project n. 211956. CPU time at CINECA has been granted by CNR-INFM.

References

[1] P. Hohenberg and W. Kohn, Phys. Rev. **136**, B864 (1964).
[2] W. Kohn and L. J. Sham, Phys. Rev. **140**, A1133 (1965).
[3] L. Hedin, Phys. Rev. **139**, A796 (1965).
[4] For a review see for example G. Onida, L. Reining, and A. Rubio, Rev. Mod. Phys. **74**, 601 (2002).
[5] D. C. Elias, R. R. Nair, T. M. G. Mohiuddin, S. V. Morozov, P. Blake, M. P. A. C. Ferrari, D. W. Boukhvalov, M. I. Katsnelson, A. K. Geim, and K. S. Novoselov, Science **323**, 610 (2009).
[6] M. van Schilfgaarde, T. Kotani, and S. Faleev, Phys. Rev. Lett. **96**, 226402 (2006).
[7] M. Shishkin and G. Kresse, Phys. Rev. B **75**, 235102 (2007).
[8] L. Hedin, J. Phys.: Condens. Matter **11**, R489 (1999).
[9] O. Pulci, M. Marsili, E. Luppi, C. Hogan, V. Garbuio, F. Sottile, R. Magri, and R. Del Sole, Phys. Status Solidi B **242**, 2737 (2005).
[10] P. Giannozzi, S. Baroni, N. Bonini, M. Calandra, R. Car, C. Cavazzoni, D. Ceresoli, G. L. Chiarotti, M. Cococcioni, I. Dabo, A. Dal Corso, S. de Gironcoli, S. Fabris, G. Fratesi, R. Gebauer, U. Gerstmann, C. Gougoussis, A. Kokalj, M. Lazzeri, L. Martin-Samos, N. Marzari, F. Mauri, R. Mazzarello, S. Paolini, A. Pasquarello, L. Paulatto, C. Sbraccia, S. Scandolo, G. Sclauzero, A. P. Seitsonen, A. Smogunov, P. Umari, and R. M. Wentzcovitch, J. Phys.: Condens. Matter **21**, 395502 (2009).
[11] M. Bockstedte, A. Kley, J. Neugebauer, and M. Scheffler, Comput. Phys. Commun. **107**, 187 (1997), http://www.fhi-berlin.mpg.de/th/fhi98md/.
[12] R. W. Godby, M. R. Schlüter, and L. J. Sham, Phys. Rev. B **35**, 4170 (1987).
[13] M. S. Hybertsen and S. G. Louie, Phys. Rev. B **34**, 5390 (1986).
R. W. Godby, R. J. Needs, Phys. Rev. Lett. **62**, 1169 (1989).
[14] L. Perdigao, D. Deresmes, B. Grandidier, M. Dubois, C. Delerue, G. Allan, and D. Stievenard, Phys. Rev. Lett. **92**, 216101 (2004).
[15] GW corrections to the DFT–LDA surface states of Si(001) have been calculated using a slab of six silicon layers with hydrogen passivating the bottom surface. The screening and the correlation part of the self-energy have been calculated using 13 *k*-points in the irreducible part of the Brillouin Zone, 797 plane waves and 800 empty bands. The exchange part of the self-energy has been calculated using 3161 plane waves.
[16] M. Rohlfing, P. Krüger, and J. Pollmann, Phys. Rev. B **52**, 1905 (1995).
[17] J. E. Northrup, Phys. Rev. B **47**, 10032 (1993).
[18] G. Bauer and W. Richter, Optical Characterization of Epitaxial Semiconductor Layers (Springer-Verlag, Berlin/Heidelberg, 1996).
[19] L. Kipp, D. K. Biegelsen, J. E. Northrup, L. E. Swartz, and R. D. Bringans, Phys. Rev. Lett. **76**, 2810 (1996).
[20] A. Bagchi, R. G. Barrera, and A. K. Rajagopal, Phys. Rev. B **20**, 4824 (1979).
[21] R. Del Sole, Solid State Commun. **37**, 537 (1981).
[22] F. Manghi, R. Del Sole, A. Selloni, and E. Molinari, Phys. Rev. B **41**, 9935 (1990).
[23] M. Marsili, N. Witkowski, O. Pulci, O. Pluchery, P. L. Silvestrelli, R. Del Sole, and Y. Borensztein, Phys. Rev. B **77**, 125337 (2008).
[24] P. L. Silvestrelli, O. Pulci, M. Palummo, R. Del Sole, and F. Ancilotto, Phys. Rev. B **68**, 235306 (2003).
[25] In the description of optical spectra is very important to mention that in the presence of strong excitonic effects, i.e. the effects of the interaction between the excited electron and hole, it is mandatory to go beyond a single-QP description in order to improve the agreement with the experiments.
[26] J. M. Carpinelli, H. H. Weitering, M. Bartkowiak, R. Stumpf, and E. W. Plummer, Phys. Rev. Lett. **79**, 2859 (1997).
[27] J. Avila, A. Mascaraque, E. G. Michel, M. C. Asensio, G. LeLay, J. Ortega, R. Perez, and F. Flores, Phys. Rev. Lett. **82**, 442 (1999).
[28] F. Ronci, S. Colonna, S. D. Thorpe, and A. Cricenti, Phys. Rev. Lett. **95**, 156101 (2005).
[29] R. I. G. Uhrberg and T. Balasubramanian, Phys. Rev. Lett. **81**, 2108 (1998).
[30] L. Jurczyszyn, J. Ortega, R. Perez, and F. Flores, Surf. Sci. **482–485**, 1350 (2001).
[31] J. S. Okasinski, C. Y. Kim, D. A. Walko, and M. J. Bedzyk, Phys. Rev. B **69**, 041401(R) (2004).
[32] O. Bunk, J. H. Zeysing, G. Falkenberg, R. L. Johnson, M. Nielsen, M. M. Nielsen, and R. Feidenhans'l, Phys. Rev. Lett. **83**, 2226 (1999).
[33] M. E. Davila, J. Avila, M. C. Asensio, and G. Le Lay, Phys. Rev. B **70**, 241308(R) (2004).
[34] Y. Fukaya, A. Kawasuso, and A. Ichimiya, Surf. Sci. **600**, 4086 (2006).
[35] T. L. Lee, S. Warren, B. C. C. Cowie, and J. Zegenhagen, Phys. Rev. Lett. **96**, 046103 (2006).
[36] R. I. G. Uhrberg, H. M. Zhang, and T. Balasubramanian, Phys. Rev. Lett. **85**, 1036 (2000).
[37] A. Tejeda, R. Cortes, J. Lobo-Checa, C. Didiot, B. Kierren, D. Malterre, E. G. Michel, and A. Mascaraque, Phys. Rev. Lett. **100**, 026103 (2008).
[38] I. Yi, R. Nishi, Y. Sugimoto, and S. Morita, Appl. Surf. Sci. **253**, 3072 (2007).
[39] R. Pérez, J. Ortega, and F. Flores, Phys. Rev. Lett. **86**, 4891 (2001).
[40] G. Ballabio, G. Profeta, S. de Gironcoli, S. Scandolo, G. E. Santoro, and E. Tosatti, Phys. Rev. Lett. **89**, 126803 (2002).
[41] A. V. Melechko, J. Braun, H. H. Weitering, and E. W. Plummer, Phys. Rev. B **61**, 2235 (2000).
[42] G. Profeta and E. Tosatti, Phys. Rev. Lett. **98**, 086401 (2007).
[43] Norm-conserving LDA pseudopotentials have been employed, but ultrasoft gradient-corrected pseudopotentials have also been tested, giving comparable results. A kinetic energy cutoff of 12 Ry, increased to 20 Ry for convergence checking, has been used in the expansion of wave functions in a plane-wave basis set. The 3×3 surface Brillouin zone (SBZ) has been sampled by a uniform mesh of 15×15 *k*-points. Tests calculations using ultra-soft pseudopotentials

with the Sn 4d levels explicitly included as valence electrons have not given appreciable differences.
[44] S. de Gironcoli, S. Scandolo, G. Ballabio, G. Santoro, and E. Tosatti, Surf. Sci. **454–456**, 172 (2000).
[45] J. Tersoff and D. R. Hamann, Phys. Rev. B **31**, 805 (1985).
[46] In the GW calculations, the same mesh of k-points has been used as for DFT. The screening and the correlation part of the self-energy has been evaluated using 600 bands and 1087 plane waves. The exchange part of the self-energy has been calculated using 12993 plane waves.
[47] A. Selloni, P. Carnevali, E. Tosatti, and C. D. Chen, Phys. Rev. B **31**, 2602 (1985).
[48] P. Gori, F. Ronci, S. Colonna, A. Cricenti, O. Pulci, and G. Le Lay, Europhys. Lett. **85**, 66001 (2009).
[49] S. Colonna, F. Ronci, A. Cricenti, and G. Le Lay, Phys. Rev. Lett. **101**, 186102 (2008).
[50] A. K. Geim, Science **324**, 1530 (2009).
[51] S. Ryu, M. Y. Han, J. Maultzsch, T. F. Heinz, P. Kim, M. L. Steigerwald, and L. E. Brus, Nano Lett. **8**, 4597 (2008).
[52] J. O. Sofo, A. S. Chaudhari, and G. D. Barber, Phys. Rev. B **75**, 153401 (2007).
[53] J. P. Perdew, K. Burke, and M. Ernzerhof, Phys. Rev. Lett. **77**, 3865 (1996).
[54] DFT calculations for the geometry have been performed using an energy cut-off of 50 Ry, a mesh of $12 \times 12 \times 1$ *k*-points and approximately 20 Å of vacuum between the sheets, for both graphane and graphene.
[55] S. B. Legoas, P. A. S. Autreto, M. Z. S. Flores, and D. S. Galvão, http://arxiv.org/abs/0903.0278.
[56] GW calculations on graphane have been performed using 1773 plane waves, 300 bands, and a mesh of $12 \times 12 \times 1$ *k*-points.
[57] The optical spectrum of graphene has been calculated using a uniform mesh of $200 \times 200 \times 1$ *k*-points in the BZ. For graphane, a mesh of $50 \times 50 \times 1$ resulted to give already well converged results. A broadening of 0.1 eV has been applied.
[58] L. Yang, J. Deslippe, C. H. Park, M. L. Cohen, and S. G. Louie, Phys. Rev. Lett. **103**, 186802 (2009).